Kinetics and Mechanism of the Oxidation of Carbon Monoxide on CoO- α -Fe_2O_3 Catalysts

Keu Hong Kim* and Jae Shi Choi

Department of Chemistry, Yonsei University, Seoul 120.

Young Bae Kim

Department of Chemistry, Konkuk University, Seoul 133. *Received June 22, 1987*

The oxidation of carbon monoxide by gaseous oxygen on 0.53, 1.02, and 1.51 mol % CoO-doped -Fe_2O_3 catalysts has been investigated in the temperature range from 340 to 480°C under various CO and O_2 partial pressures. The oxidation rates have been correlated with 1.5-order kinetics; the 0.5-order with respect to O_2 and the first-order with respect to CO. In the above temperature range, the activation energy is 0.34 ± 0.01 eV·mol^{-1}. The electrical conductivity of 0.53, 1.02, and 1.51 mol % CoO-doped α-Fe_2O_3 has been measured at 350°C under various P_{CO} and P_{O_2}. From the conductivity data it was found that O_2 was adsorbed on Vö formed by doping with CoO, while CO appeared essentially to be chemisorbed on the lattice oxygen of the catalyst surface. The proposed oxidation mechanism and the dominant defect were supported by the agreement between the kinetic data and conductivities.

Introduction

The catalytic activity of ZnO in the oxidation of CO is mainly dependent on the amount of excess Zn_i in ZnO[1]. On the other hand, the oxidation of SO_2 is due to an oxygen vacancy of n-type TiO_2[2], and not to interstitial Ti ions which are observed by the conductivity measurements at increased temperatures above 630°C[3]. From the ir study by Tascon *et al*[4], CO_3^{2-} intermediate was observed in the oxidation of CO on $LaCoO_3$ catalyst at 100-150°C. This observation of CO_3^{2-} intermediate suggests that the molecular carbon monoxide is adsorbed on lattice oxygen. Similar result was deduced from the conductivity measurements of α-Fe_2O_3 under gaseous SO_2; conductivity increased with increasing P_{SO_2}, indicating that the lattice oxygen was a possible site for SO_2 adsorption and the SO_3^- intermediate thus formed acted as an electron donor[5].

The oxygen species such as O^- ion adsorbed on ZnO, SnO_2 and TiO_2 is directly identified by means of esr spectroscopy. From the temperature programmed desorption technique[6], it was observed that the highest detector response for desorbed oxygen appeared in α-Fe_2O_3 at 200-400°C among the 9 oxides such as NiO, CuO, SnO_2, etc. This implies that the adsorption site for molecular oxygen in α-Fe_2O_3 is more easily formed than in other metal oxides, while the number of site s could be altered by the sample preparation method.

The purpose of this work is to investigate how the catalytic activity of α-Fe_2O_3 varies with the doping with CoO and how the catalytic structure formed possibly by this doping affects the oxidation mechanism of carbon monoxide.

Experimental

Material Preparation. *(a) Pure α-Fe_2O_3.* α-Fe_2O_3 powder was prepared by the following steps[7]: $Fe(NO_3)_3 \cdot 9H_2O$ was dissolved in 6% NH_4OH and allowed to react with continuous stirring for 50 min. The precipitate was filtered, washed 10 times with distilled warm water, and then dried at 80°C. The dried $Fe(OH)_3$ powder was then heated for 10 h at 220°C. The resulting powder was a reddish brown α-Fe_2O_3 confirmed by X-ray technique. The chemical reactions involved are $Fe(NO_3)_3 \cdot 9H_2O + 3NH_4OH \rightarrow Fe(OH)_3 + 3NH_4NO_3 + 9H_2O$ and $2Fe(OH)_3 \rightarrow \alpha\text{-}Fe_2O_3 + 3H_2O$. The main impurities of α-Fe_2O_3 were Ca, Cu, Mn, Co, etc. of total 83 ppm analyzed by aas.

(b) 0.53, 1.02, and 1.51 mol % CoO-doped α-Fe_2O_3 Catalysts. The prepared α-Fe_2O_3 powder from the above procedure[7] and the CoO powder obtained from Johnson Matthey Co. (99.99% purity) were used for the preparation of CoO-doped α-Fe_2O_3 catalysts. Appropriate weights of the oxide powders were mixed in ethanol solution and stirred for 72 h to obtain a homogeneous dispersion. The mixture was then filtered and dried at 150°C. This mixed powder was put on a covered platinum crucible, placed in a preheated furnace, and sintered in air pressure at 800°C for 10 h and then slowly cooled to room temperature. The sintered sample was annealed at 1350°C for 48 h and then cooled rapidly to room temperature. For the identification of crystalline phase, X-ray technique was performed, and doping level of each sample was confirmed by atomic absorption spectroscopy. Each sample of 100-160 mesh was found to have a Blain test surface area of 5.54 m^2/g, nearly independent of doping level. *(c) 0.53, 1.02, and 1.51 mol % CoO-doped α-Fe_2O_3 pellets.* For the conductivity measurements, some of the powder mixtures were compressed under a pressure of 1.2 tons/cm^2 into pellets and sintered at 800°C for 10 h and then slowly cooled to room temperature. The sintered pellet was annealed at 1350°C for 48 h and then cooled rapidly to room temperature. After cooling, the pellet was given a light abrasive polish onto surfaces until the voids on the surface were fully eliminated. The pellet was then cut into a rectangular shape with dimensions of 1.0 × 0.7 × 0.2 cm and polished again. The pellet was etched with several etching solutions such as $(NH_4)_2S_2O_8$ before conductivity measurements. *(d) Carbon monoxide and Oxygen gases.* CO was prepared by the method described in the Weinhouse report[8]. Commercial O_2(99.98%, Matheson Gas Products) was used for kinetic and conductivity measurements. CO and O_2 were purified by passing them over glass wool, P_2O_5, and $CaCl_2$. This purification was found to give CO and O_2 sufficiently free of catalytic poisons for catalytic reactions.

Rate and Conductivity Measurements. *(a) The reaction rate measurements.* The rates of CO oxidation were measured in a completely closed Pyrex chamber with a total volume of 146 m*l*. The catalyst was etched with dilute HNO_3 and $(NH_4)_2S_2O_8$, washed with distilled and deionized warm water, and then dried in a vacuum desiccator. The powder catalyst was placed in the Pyrex chamber and sintered at 400°C under 10^{-3} Torr for 50 min, and then cooled to room temperature before reactants CO and O_2 were introduced. The Pyrex chamber was then placed in an electric furnace maintained at a constant temperature controlled within ±0.5°C. In each run, 0.5 g of catalyst was distributed uniformly in the Pyrex chember bed. The initial pressure of the stoichiometric $2CO + O_2$ mixture was 75 Torr at each reaction temperature. Conversion of CO was monitored by the pressure change at regular time intervals and read by scaled microscope. To investigate the partial orders of CO and O_2, the P_{CO} and P_{O_2} were varied at 400°C. The product CO_2 was confirmed by gas chromatography at regular time intervals. *(b) The conductivity measurements.* The conductivity measurement circuitry and the four-probe model are previously described[9,10]. The details of the experimental apparatus, instruments, and calculations of measured conductivity have been given in the previous papers[9,10]. Measurements of electrical conductivity were performed according to Valdes' technique which has been briefly described in previous papers[9,10]. This technique has also been employed to measure the electrical conductivity of other metal oxide semiconductors, e.g. Tm_2O_3[11], $SrTiO_3$: Ni/CO-reduced $SrTiO_3$: Ni[12], Sm_2O_3[13], H_2-reduced rutile, Fe_2O_3: Ni[14], etc. The current through the sample was maintained from 10^{-7}-10^{-2} A by rheostat and the potential across the inner two probes was maintained between 0.3 and 1.7 V. The various P_{CO} and P_{O_2} were established using pure CO and O_2 obtained from above methods. The pressures of CO and O_2 were read on a Pirani gauge and Mcleod gauge, respectively.

Results

Determining the Reaction Order. *(a) The total order.* The direct data plots were employed to determine the total order. The reaction rates of CO oxidation on CoO-α-Fe_2O_3 catalysts are found to closely obey a $-(dp/dt) = kP^{1.5}_{CO+O_2}$ with respect to the total pressure ($P_{CO}+P_{O_2} = 75$ torr) in the reaction temperature range 340-480°C.

Figure 1 shows $10^3(P^{-0.5}\text{-}P_0^{-0.5})$ plotted against time at various temperatures, the linearity confirming 1.5-order kinetics on α-Fe_2O_3 doped with 0.53 mol % CoO. Figure 2 shows 500 ($P^{-0.5}\text{-}P_0^{-0.5}$) vs. time for α-Fe_2O_3 doped with various mol % CoO at 420°C, the linearity also confirming 1.5-order kinetics. The values of the rate constants in Table 1 obtained from the slopes of plots of concentration versus time are found to be compatible with the Arrhenius equation. The logarithms of the rate constants plotted against the reciprocals of the temperature are shown in Figure 3. The slopes of the lines are calculated from the plots, and the activation energies for three samples are similar with 0.34 ± 0.01 eV. *(b) The partial orders.* The changes in initial reactant concentrations were used to determine the partial orders. The ratio of P_{CO} and P_{O_2} is varied to measure the oxidation rates of CO. Table 2 shows the reaction rates for three samples within the same reaction temperature interval (400°C). The powers are

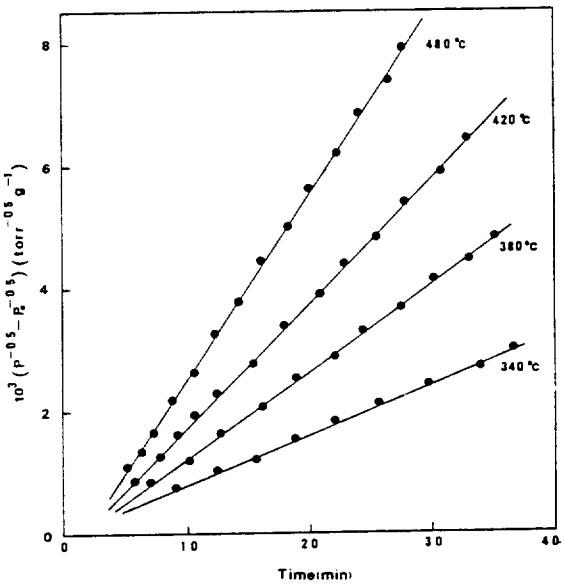

Figure 1. Oxidation rates of carbon monoxide on 0.53 mol % CoO-α-Fe_2O_3 at various temperatures. P_{CO} = 50 torr; P_{O_2} = 25 torr; catalyst = 1g (100-160 mesh); P_0, total initial pressure; P, total pressure.

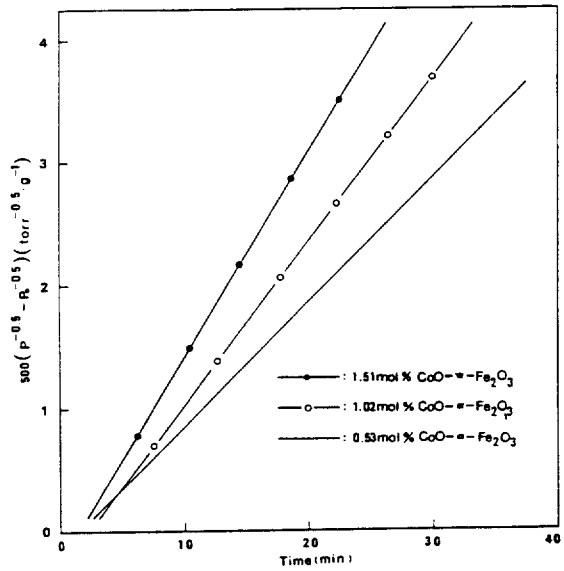

Figure 2. Comparative rates of CO oxidation on various CoO-α-Fe_2O_3 at 420°C. P_{CO} = 50 torr; P_{O_2} = 25 torr; each catalyst = 1 g(100-160 mesh); P_0, total initial pressure; P, total pressure.

evaluated for P_{CO} and P_{O_2} from the data in Table 2. The partial orders of CO and O_2 are found to be first-order and half-order, respectively, independent of CoO doping level. The rate law which represents the experimental data for α-Fe_2O_3 doped with three different mol % CoO in the reaction temperature range 340-480°C is given by $r = kP_{CO}\cdot P_{O_2}^{0.5}$. *(c) The effect of CoO mol % on reaction rates.* The catalytic activity was measured as a function of CoO mol % on the oxidation of CO. Figure 4 shows the rate of CO oxidation versus CoO mol % under two typical partial pressures of CO and O_2 at 400°C. The reaction rate increases with increasing CoO doping level at two different stoichiometric total pressures. The slope in the plot of v × 10 vs. CoO mol % at ($P_{CO}+P_{O_2}$) = 75 torr is larger than that at ($P_{CO}+P_{O_2}$) = 38 torr at

Table 1. Temperature Dependence of Specific Rates of CO Oxidation on CoO-α-Fe_2O_3 Catalysts

Catalysts	T°C	k(torr$^{-0.5}$, min^{-1}, g^{-1})
	340	8.00×10^{-5}
0.53 mol%	380	1.43×10^{-4}
CoO-α-Fe_2O_3	420	2.00×10^{-4}
	480	3.00×10^{-4}
	340	1.27×10^{-4}
1.02 mol %	380	1.80×10^{-4}
CoO-α-Fe_2O_3	420	2.67×10^{-4}
	480	3.66×10^{-4}
	340	1.64×10^{-4}
1.51 mol %	380	2.50×10^{-4}
CoO-α-Fe_2O_3	420	3.33×10^{-4}
	480	5.20×10^{-4}

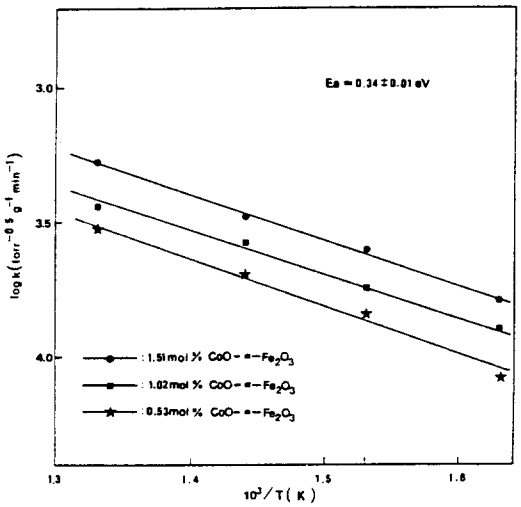

Figure 3. Arrhenius plots for the rates of CO oxidation on various CoO-α-Fe_2O_3 catalysts.

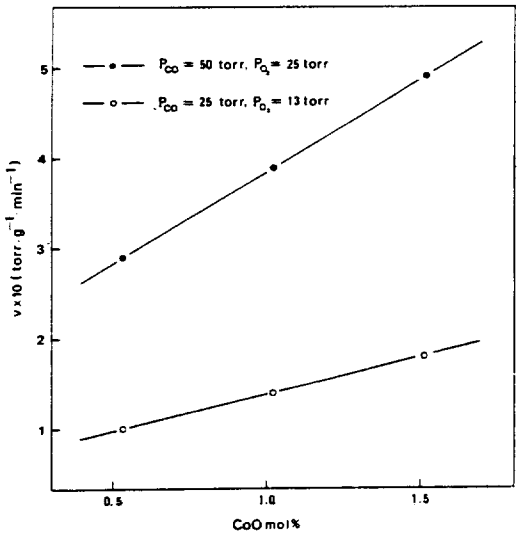

Figure 4. The rate of CO oxidation vs. CoO mol % under various partial pressures of carbon monoxide and oxygen at 400°C.

constant temperature, showing the increased reaction rate under higher stoichiometric total pressure. *(d) The conductivity data.* To investigate the conductivity variation of α-Fe_2O_3 doped with various mol % CoO under P_{CO}'s and P_{O_2}'s, the conductivities were measured as a function of time. Figure 5 shows the conductivity changes of three samples under various partial pressures of CO. The conductivity increases with increasing mol % CoO at same P_{CO} and also increases with increasing P_{CO} for constant doping level. Figure 6 shows P_{O_2} dependence of conductivity for various mol % CoO-α-Fe_2O_3 at three typical P_{O_2}'s. The conductivity decreases with increasing P_{O_2}'s and also decreases with increasing mol % CoO at constant P_{O_2} and temperature. As can be seen in Figures 5 and 6, the equilibrium time of conducti-

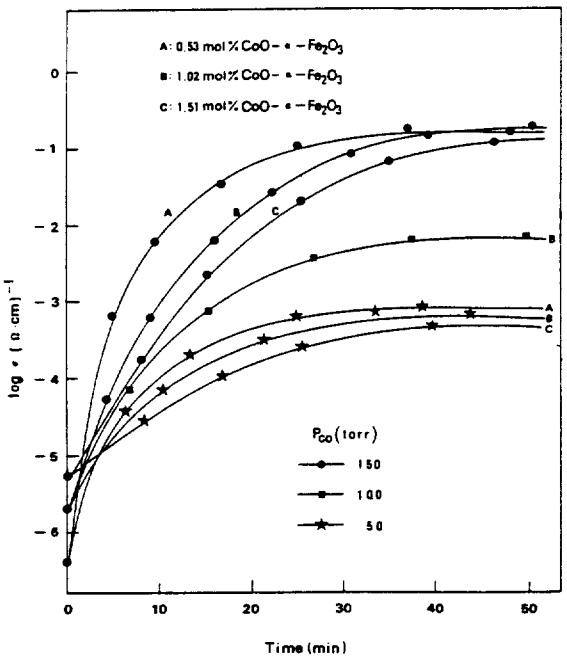

Figure 5. P_{CO} dependences of conductivity for various mol % CoO-α-Fe_2O_3 as a function of time at 350°C.

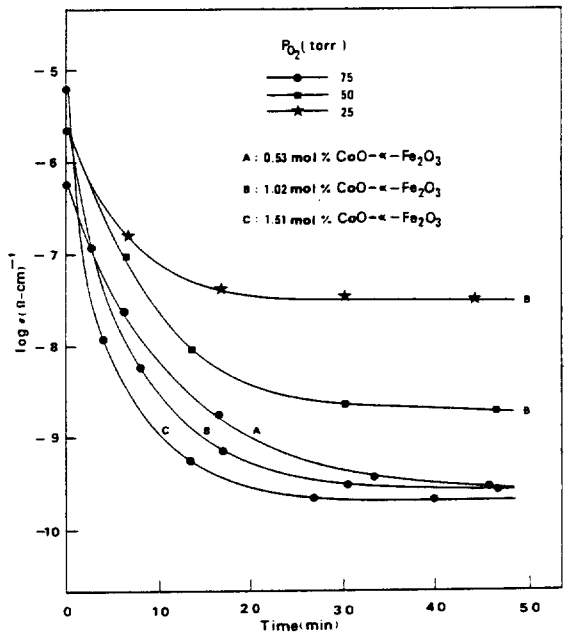

Figure 6. P_{O_2} dependences of conductivity for various mol % CoO-α-Fe_2O_3 as a function of time at 350°C.

Table 2. P_{CO} and P_{O_2} Dependences of Reaction Rate on the Oxidation of Carbon Monoxide over Various CoO-α-Fe_2O_3 Catalysts at 400°C

Catalysts	P_{CO}	P_{O_2}	r(torr, g^{-1}, min^{-1})
0.53 mol % CoO-α-Fe_2O_3	50	25	0.29
	50	13	0.21
	25	13	0.10
1.02 mol % CoO-α-Fe_2O_3	50	25	0.39
	50	14	0.29
	25	13	0.14
1.51 mol % CoO-α-Fe_2O_3	50	25	0.49
	50	13	0.35
	25	14	0.18

vity under P_{CO} is different from that under P_{O_2}: the equilibrium for P_{O_2} reaches faster than that for P_{CO}.

Discussion

The rate expression ($r = kP_{CO}P_{O_2}^{0.5}$) indicates that the inhibition effect of CO_2 is not involved in the elementary reactions on the CoO-α-Fe_2O_3 catalysts investigated in this work. The overall reaction order for CO oxidation on CoO-α-Fe_2O_3 catalysts agrees well with the total order of SO_2 oxidation on n-type TiO_2 catalysts[2] within the experimental error. However, the total order is different from that on a p-type NiO catalyst[2]. Moreover, the partial orders for the present catalysts differ from those ($r = kP_{SO_2}^{0.2}P_{O_2}^{0.8}$) observed for a NiO catalyst[2]. Matsuura *et al.*[11] reported that the rate law is $r = kP_{CO}\cdot P_{O_2}^{1/2}$ on n-type ZnO. The present data on n-type CoO-α-Fe_2O_3 catalysts fit well with the total and partial orders observed by Matsuura *et al.*[11] on n-type ZnO which are different from $r = kP_{O_2}^{1/2}$ observed by Amigues and Teichner[12] on ZnO catalyst, and $r = kP_{CO_2}^{1/2}$ on pure ZnO or $r = kP_{CO}^{0.7}$ on Li-and In-doped ZnO catalysts[13]. The reaction rates observed by Matsuura *et al*[11] and the present work are contrasts greatly to the rates observed by Amigues and Teichner[12] and by Chizhikova[13]; the overall reaction of Amigues and Teichner is independent of CO pressure, while chizhikova's[13] is independent of O_2 pressure over the ZnO catalyst. The rate law whose rate is independent of CO pressure was observed on H_2-reduced α-Fe_2O_3 doped with NiO[14]; $r = kP_{O_2}^{1/2}$ as same as Amigues and Teicher's[12]. The inhibiting effect of carbon dioxide was observed on In_2O_3 catalyst[15], but it did not appear on CoO-α-Fe_2O_3.

Adsorption sites from possible defects. *(a) Adsorption site for CO.* The present kinetic data shown in Table 2 indicate that the overall reaction rates are dependent on the partial pressures of CO and O_2. This result means that the reactants CO and O_2 are adsorbed on possible defects of CoO-α-Fe_2O_3 surface. The conductivity data shown in Figure 5 indicate that CO adsorption produces conduction electron; the increased P_{CO} increases the electrical conductivity and the conductivity also increases with decreasing mol % of CoO doped. The former indicates that the conduction electrons are produced by the adsorption of CO on lattice oxygen in CoO-α-Fe_2O_3 surface. On the other hand, the latter shows that the conduction electrons produced by CO adsorptions decrease with increasing mol % of CoO doped, indicating the elimination of lattice oxygen by CoO doping. This reduction of lattice oxygen is due to the formation of oxygen vacancy. Based on the principle of controlled valency, x oxygen vacancies are produced by the reaction

$$CoO + \alpha - Fe_2O_3 \longrightarrow Co^{2+}Fe_{2-2x}^{3+}Fe_{2x}^{2+}O_{4-x}^{2-} + \frac{x}{2}O_2 + 2xe' + xV_{\ddot{O}} \quad (1)$$

where V_O is an oxygen vacancy formed by CoO doping. The increased mol % CoO moves the reaction (1) to the right and the concentration of oxygen vacancy is increased, resulting in decrease of lattice oxygen. The two different kinds of conductivity data with respect to P_{CO} and mol % CoO lead us to believe that the adsorption site for CO is lattice oxygen on CoO-α-Fe_2O_3 surface. *(b) Adsorption site for O_2.* The conductivities as shown in Figure 6 decrease with increasing P_{O_2} and mol % CoO. The increased conductivity in increased doping level shows that the concentration of conduction electron increases with increasing CoO doping according to the reaction(1). This is the case of conductivities with zero P_{O_2} (time = 0) in Fig. 6. However, the conductivity decreases with increasing mol % CoO at constant P_{O_2}. This result indicates that the increased doping level produces increased adsorption site of O_2. The more adsorption of O_2 on increased adsorption site occurs, the more electron is consumed. If the oxygen vacancy produced by reaction(1) serves as a possible adsorption site for O_2, the electron concentration should decrease according to the reaction

$$O_2(g) + 2e^- \overset{K_1}{\rightleftharpoons} 2O^-_{(ads)} \quad (2)$$

where e^- is a conduction electron trapped at an oxygen vacancy produced by CoO doping. As shown in Figure 6, the conductivity decreases with increasing P_{O_2} at constant doping level. This is consistent with the reaction(2); the increased P_{O_2} moves the reaction(2) to the right hand side. The conductivity data in Figure 6 leads us to believe that the adsorption site for O_2 is oxygen vacancy which is produced by the doping of CoO and has two trapped electrons($V_{\ddot{O}}$-$2e'$).

Reaction Mechanism. The kinetic data in Figure 1 and Table 2 support that CO may be adsorbed as a molecular state, while O_2 does as an atomic one, since the rate expression ($r = KP_{CO}P_{O_2}^{1/2}$) includes first-order with respect to CO and half-order with respect to O_2. As indicated above, if the adsorption site for CO is lattice oxygen, one can write following reaction where $CO^-_{2(ads)}$ is the molecular CO adsorbed on

$$CO(g) + O^{2-}_{(latt)} \overset{K_2}{\rightleftharpoons} CO^-_{2(ads)} + e^- \quad (3)$$

the lattice oxygen and e^- is conduction electron. As shown in Figure 5, the increasing P_{CO} moves the equilibrium to the right, producing conduction electron. The $CO^-_{2(ads)}$ is possible species, since CO_2 is not observed by gas chromatography. The reaction(3) is consistent with the conductivity data in Fig. 4 and kinetic data in Figure 1 and 4 and in Table 2.

The 1/2 order with respect to oxygen molecule and the conductivity data in Figure 6 support that O_2 is adsorbed on an oxygen vacancy and then dissociate into atomic species; an O_2 is adsorbed on an $V_{\ddot{O}}$ with two trapped electrons, and then accepts two electrons into the weakly adsorbed oxygen $\pi(\pi^*_{2p})$ orbital. As a result, the oxygen bond is reduced from double bond to single bond. From this reduction of the bond order, the weakly adsorbed species has a primary vibrational frequency characteristic of a peroxo($O^{2-}_{2(ads)}$) species, indicating an O-O single bond. The existence of $O^{2-}_{2(ads)}$ in the

adsorbed state can be supported by the conductivity data in Figure 5, since the π_g orbitals of molecular O_2 accept the conduction electrons trapped at $V_{\ddot{O}}$. On the other hand, the kinetic data should not agree with $O^{2-}_{2(ads)}$, since the rate law, *i.e.*, the half-order with respect to oxygen, satisfies with atomic oxygen species. The conductivity and kinetic data support that $O^-_{(ads)}$ is a reasonable species at investigated temperatures, indicating the reaction(2) is an elementary reaction included in the oxidation process of CO.

The kinetic data in Tables 1 and 2 and the conductivity data of Figures 5 and 6 support that the following elementary reaction should be included in the overall reaction. From the

$$O^-_{(ads)} + CO^-_{(ads)} \xrightarrow{k'} O^{2-}_{(lattice)} + CO_2\,(g) \qquad (4)$$

kinetic data in Figures 2 and 4, and the conductivity data in Figures. 5 and 6, the adsorption *rate* of CO on lattice oxygen (equilibrium(3)) is lower than that of O_2 on an $V_{\ddot{O}}$ (equilibrium(2)) at constant temperature, P_{O_2} and catalyst. Therefore, the equilibrium(3) must be the rate-determining step.

The experimental rate law, $r = kP_{CO}\cdot P_{O_2}^{1/2}$ should be derived from the above mechanism, if the elementary reactions (2)-(4) are true in the oxidation process of CO. In equilibrium (2) $(O^-) = K_1^{1/2}P_{O_2}^{1/2}(e^-)$, and $(CO_2^-) = K_2P_{CO}(O^{2-})/(e^-)$ in equilibrium(3) with omissions of the obvious subscripts. The rate of elementary reaction(4) which produces CO_2 is $dP_{CO_2}/dt = k'(CO_2^-)\,(O^-)$. Substituting $(O^-) = K_1^{1/2}P_{O_2}^{1/2}(e^-)$ and $(CO_2^-) = K_2P_{CO}(O^{2-})/(e^-)$ into this rate law, the overall rate is consistent with the experimentally observed rate law, indicating $k = k'\cdot K_2K_1^{1/2}$ and $(O^{2-}_{latt}) \simeq$ constant. The elementary reactions (2), (3), and (4) are possibly suggested as the reaction mechanism, since the observed rate law can be derived from above elementary reactions.

Acknowledgement. The authors are grateful to the Korean Science and Engineering Foundation for financial support and to Professor S. H. Lee for helpful discussion.

References

1. J. S. Choi and B. W. Kim, *Bull. Chem. Soc. Jpn.*, **46**, 21 (1973).
2. J. S. Choi, K. H. Kim, and S. R. Choi, *Int. J. Chem. Kinet.* **9**, 489 (1977).
3. J. S. Choi and K. H. Kim, *J. Phys. Chem.* **80**, 666 (1976).
4. J. M. D. Tascon, J. L. Garcia, and L. G. Tejuca, *Z. Phys. Chem.* **B 124**, 249 (1981).
5. K. H. Kim and J. S. Choi, *J. Phys. Chem.* **85**, 2447 (1981).
6. M. Iwamoto, Y. Yoda, N. Yamazoe, and T. Seiyama, *J. Phys. Chem.* **82**, 2564 (1978).
7. J. P. Reymond, P. Meriaudeau, and S. J. Teichner, *J. Catalysis* **75**, 39 (1982).
8. S. Weinhouse, *J. Am. Chem. Soc. Commun. Ed.* **70**, 442 (1948).
9. J. S. Choi, H. Y. Lee, and K. H. Kim, *J. Phys. Chem.* **77**, 2430 (1973).
10. J. S. Choi, Y. H. Kang, and K. H. Kim, *J. Phys. Chem.* **81**, 2208 (1977).
11. I. Matsuura, T. Kubokawa, and O. Toyama, Nippon Kagaku Zasshi **88**, 830 (1967).
12. P. Amigues and S. J. Teichner, *Discuss. Faraday Soc.*, **41**, 362 (1966).
13. G. I. Chizhikova, *Kinet. Katal.* **7**, 660 (1966).
14. Don. Kim, K. H. Kim, and J. S. Choi, Unpublished paper (1987).
15. S. H. Lee, G. Heo, K. H. Kim, and J. S. Choi, *Int. J. Chem. Kinet.*, **19**, 1 (1987).

Solvolysis of 2-Phenylethyl Benzenesulfonates in Methanol-Water Mixtures

Goang Lae Han, Jin Ha Park

Department of Chemistry, Chonbuk National University, Chonju 520

Ikchoon Lee*

**Department of Chemistry, Inha University, Inchon 160, Re eived June 24, 1987*

Solvolyses of 2-phenylethyl benzenesulfonates have been studied in methanol-water mixtures. Cross interaction constants, ρ_{YZ}, between substituents Y in the substrate and Z in the leaving group indicated somewhat closer distance between the two substituents than expected for the reaction system, which supported the involvment of phenyl group assisted pathway in the solvolysis. A smaller magnitude of ρ_{YZ} for MeOH was interpreted as the enhencement of solvent assisted pathway since MeOH is more nucleophilic than H_2O. Other selectivity parameters, Winstein coefficient m, Hammett's ρ_Y^+ and ρ_Z, as well as activation parameters supported the participation of aryl assisted and aryl unassisted pathways in the S_N2 process of the solvolysis reaction.

Introduction

2-Phenylethyl derivatives have attracted considerable attention of physical organic chemists ever since phenonium ions (I) were first proposed as solvolysis intermediates in solvolyses of 2-arylalkyl systems.[1] It has since been well established that solvolyses of 2-arylalkyl systems proceed through discrete aryl assisted(k_Δ) and/or aryl unassisted(k_s)